



Distinguishing skin cancer cells and normal cells using electrical impedance spectroscopy



Fan Zhang*, Tongyu Jin, Qingqing Hu, Pingang He

School of Chemistry and Molecular Engineering, East China Normal University, Shanghai 200241, PR China

ARTICLE INFO

Keywords:

Electrical impedance spectroscopy
Skin cancer cells
Skin normal cells
Cell proliferation
Equivalent circuits

ABSTRACT

In this study, distinguishing skin cancer cells (A431) and normal cells (HaCaT) was achieved using electrical impedance spectroscopy (EIS) with a novel developed device. The proliferation behaviors of the two cell types during a culture period of 5 days were characterized by the normalized impedance measured at 1465 Hz with simultaneous microscopic imaging for assistance. By fitting to the established equivalent circuits, A431 cells generated smaller resistance (R_c) values with smaller increasing variation, and comparable capacitance (C_c) values with similar decreasing variation compared with HaCaT cells. Moreover, C_c values were linearly correlated to the cell number. The results indicate that these two cell types can be distinguished with EIS based on the differences in the values and variation trends of R_c and C_c during the proliferation process in a real-time and label-free manner. Our work supplies a useful analytical approach for skin cancer cell research and may facilitate the early diagnosis of skin cancer.

1. Introduction

Skin cancer is one of the most common malignancies worldwide, especially among Caucasians. In general, skin cancer includes melanoma, basal cell carcinoma (BCC) and squamous cell carcinoma (SCC). BCC and SCC are the major clinical manifestations of skin cancer, called non-melanoma skin cancer, and both of them are derived from epidermal keratinocytes. SCC is more aggressive and more likely to invade other tissues. Fortunately, if early detection and treatment are available, 90% of skin disease can be cured [1]. Thus, there is a strong demand to effectively and quickly detect skin cancer cells in the early stage.

At present, cancer detection mostly depends on pathological diagnosis, which requires sophisticated procedures and careful inspection under microscopy by highly skilled pathologists. Moreover, by the time of cancer confirmation, the cancer has often already reached a later stage. Therefore, in recent years, numerous efforts have been undertaken to explore new methods for the detection of cancer cells, including optical [2–4] and electrochemical [5–7] strategies. However, most of them could not achieve the continuous monitoring of cells with the interruption of culture process, thus impossibly providing dynamic information. Therefore, developing continuous, real-time, and non-invasive detection techniques for cancer cell discrimination are urgently needed.

Electrical impedance spectroscopy (EIS) is an analytical technique

to detect electrical properties of tissues or cells. It can capture quantitative cell information, including the resistance and the capacitance, which could be used to indicate the viability or behavior variations of cells, since there is a strong correlation between the electrical properties of cells and their physiological states [8–12]. Giaever and Keese previously employed impedance in investigating mammalian fibroblasts cultured on evaporated gold electrodes. The cells that attached and spread on the electrode had a marked effect on the impedance [13]. Since the publication of that study, EIS has been used to determine various cell behaviors [14,15], such as cell adhesion [16,17], cell proliferation [18], cell migration [19,20], wound healing [21] and cytotoxicity [22,23]. Moreover, EIS has become a novel tool to identify cancer cells and normal cells without the use of any biomarkers [24–26].

In this study, EIS was exploited to distinguish skin cancer cells (A431 cells) and normal cells (HaCaT cells) in a real-time and label-free manner. The proliferation behaviors of the two cell types were monitored by EIS with a novel impedance sensing device. To further investigate the electrical properties of cells, equivalent circuits were established to analyze cellular components, including capacitance and resistance. Moreover, the electrical properties of the two cell types were correlated to cell numbers, reflecting their proliferation behaviors. To the best of our knowledge, this report is the first to describe distinguishing skin cancer cells and normal cells based on the resistance and capacitance variations of cells in the proliferation process, which could

* Corresponding author.

E-mail address: fzhang@chem.ecnu.edu.cn (F. Zhang).

provide more precise discrimination of skin cancer cells. Our study would endorse the feasibility of using EIS in clinical trials.

2. Materials and methods

2.1. Design and fabrication of EIS device

An EIS device was designed and fabricated to simultaneously measure cell impedance and image cells. As illustrated in Fig. 1, this device consists of (from top to bottom) platinum (Pt) gauze, a cell chamber, a poly-dimethylsiloxane (PDMS) seal ring, indium tin oxide (ITO) glass and a baseboard. The cell chamber and the baseboard, made of Teflon and fabricated using micro milling with the help of Shanghai Kunbo Mould Co. Ltd., China. ITO glass (Zhuhai Kaivo Optoelectronic Technology Co. Ltd., China), was inserted into the baseboard and employed as a working electrode (WE), due to its good electrical conductivity, transparency and biocompatibility. The cell chamber, shaped as an inverted trapezoid, was positioned on the surface of ITO glass; thus, the active working electrode area was fixed at 0.28 cm². Meanwhile, the Pt gauze (Wuhan Gaosunion Technology Co. Ltd., China), with 7.06 cm² of active area, served as counter electrode (CE) and reference electrode (RE) and was placed on the top of the chamber opposite the working electrode. The counter and reference electrode were 25 times larger than the working electrode, and as a result, the impedance variation was determined mainly by the working electrode, which improved the detection sensitivity. On the other hand, the larger upper opening of the chamber is convenient to perform cell procedures, such as seeding cells and changing medium. Additionally, the design of card slot and binding post used to fix electrodes and wires, ensured the accuracy and reproducibility of impedance monitoring. To improve the sealing performance of the EIS device, a PDMS seal ring was utilized between the cell chamber and ITO glass. This seal ring was prepared by mixing PDMS base polymer and cross-linker (methylhydrosiloxane dimethylsiloxane copolymers) at the ratio of 10:1. After PDMS was thermally cured on the silicon wafer for 2 h at 80 °C, it was peeled off and drilled with a punch. The device was assembled with screws, facilitating the replacement of the working electrode and the reutilization of the device.

2.2. Cell culture

A431 (Human Epidermoid Carcinoma; skin cancer cells) and HaCaT (Human Immortal Keratinocyte Cell Line; skin normal cells) were purchased from Shanghai Bogoo Biotech Co. Ltd., China. Cells were cultured in a 5% CO₂ high-humidity atmosphere at 37 °C with minimum essential medium (MEM) containing 10% fetal bovine serum (FBS) and 1% penicillin-streptomycin (Invitrogen, China). The culture medium was changed every three days. When cells reach confluence, 0.25% trypsin/EDTA (Invitrogen, China) was used to detach the cells. After removing the trypsin solution, cells were resuspended in culture medium, and cell number and viability were evaluated by direct cell counting with trypan blue staining.

2.3. Real-time EIS monitoring of cell proliferation

Before cell seeding, the EIS device was ultrasonically washed with ethanol and deionized water for 5 min, respectively, followed by sterilization in an autoclave at 120 °C for 20 min and ultraviolet radiation for 1 h. Next, 4 mL of culture medium was added to the device and equilibrated for 10 min at 37 °C in 5% CO₂ incubator (NuAire, USA). The impedance scanning was carried out on electrochemical station IGS4030 (Guangzhou Ingsens Sensor Technology Co., Ltd., China) to obtain the background response ($Z_{\text{cell-free}}$) in a frequency range from 1 Hz to 100 kHz with a signal amplitude of 10 mV. Subsequently, cells were seeded in the device at a density of 8×10^3 cells/cm². Every 24 h, the culture medium was renewed, and the impedance spectra were recorded under the same conditions during 5 days of culturing. The change of the culture medium before each detection minimized the influence of medium ingredients on the impedance responses. All impedance spectra were recorded at 37 °C.

To eliminate the effect of the culture medium and the conductivity of ITO glass on impedance response, the impedance data were normalized by the impedance of the culture medium without cells, which could be written as normalized impedance (NI).

$$NI = \frac{Z_{\text{cell-cover}} - Z_{\text{cell-free}}}{Z_{\text{cell-free}}} \quad (1)$$

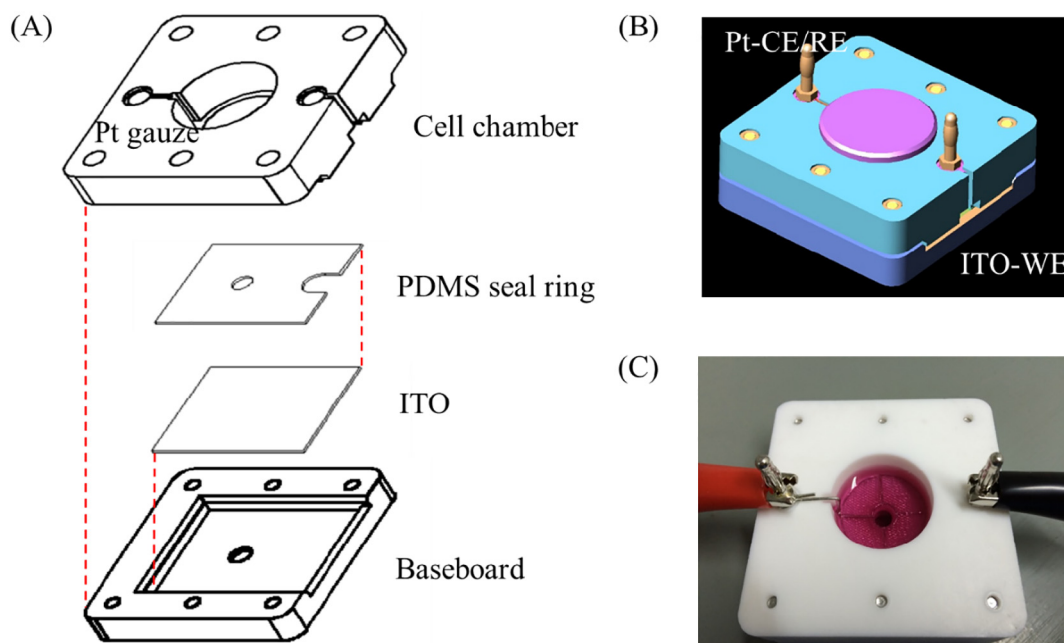


Fig. 1. (A) The construction of the EIS device: Pt gauze, cell chamber, PDMS seal ring, ITO glass and baseboard. (B) 3D illustration of the EIS device with ITO glass as working electrode and Pt gauze as counter electrode and reference electrode. (C) Photograph of the EIS device with the addition of culture medium and electrical connections.

where $Z_{\text{cell-cover}}$ and $Z_{\text{cell-free}}$ are the impedances of the system with and without cells in the device under the same conditions [8].

All impedance analyses were repeated three times, and data were expressed as the mean of the three repeated results with corresponding relative standard deviations.

2.4. Microscopic imaging

ITO glass is transparent so that the cells cultured in the device could be imaged by the inverted microscope (Olympus IX51, Japan) with a CCD camera to assist the measurement of cell proliferation behaviors. For each device, 10 images from different parts of the working electrode, covering an area of approximately $1390 \mu\text{m} \times 1045 \mu\text{m}$, were captured after impedance determination. Cell numbers were counted from the images and expressed using the mean value.

3. Results and discussion

3.1. Electrical impedance spectroscopy (EIS) monitoring of skin cancer cells (A431) and normal cells (HaCaT)

The impedance measurements were performed on ITO glass in the EIS device at the frequency range from 1 Hz to 100 kHz over a culture time of 5 days. It is known that the evaluation of cell impedance is a frequency-dependent measurement. At low frequencies ($f < 10$ Hz), the electrolyte/electrode capacitance dominates the system impedance. At high frequencies ($f > 100$ kHz), the system impedance only includes the resistance of the culture medium, electrodes and wiring. It is only in the intermediate frequency range that the system impedance is determined by the cells and their variations [27]. From the normalized impedance (NI) curves in Fig. 2A and B, it was observed that with the increase of frequency, all NI curves of both cell types first increased and later declined during the culture process. The peaks at 1465 Hz indicated a maximum difference of daily NI values during the culture processes of both A431 and HaCaT cells, and a maximum difference between these two cell types on any given day. The impedance at this frequency was the most sensitive to the associated changes during cell proliferation. Therefore, 1465 Hz was selected as the optimum frequency to distinguish A431 and HaCaT cells.

Thus, we later studied the time-dependent NI values of these two cell types at the frequency of 1465 Hz for the measurement of proliferation behaviors (Fig. 2C). Obviously, HaCaT cells presented higher NI values than A431 cells at any determination time in the culture period. Meanwhile, the NI values of the two cell types both increased with the prolongation of time; however, the increasing rates differed depending on the cell type. For A431 cells, there was a steady increase in NI value over the entire period, without an obvious difference in the change rate. However, for HaCaT cells, the NI curve could be separated into two stages with reference to the change rate. Clearly, from Day 1 to Day 3, the NI value increased sharply. In the last 2 days, the NI value showed a relatively slow increase.

To examine the proliferation behaviors of the two cell types in the respective stages, A431 and HaCaT cells on the ITO glass of the EIS device were imaged over a period of 5 days using the microscope along with the EIS determination at every 24 h of the culture process. From the microphotographs in Fig. 3A and B, it was observed that an increasing number of cells was presented as the culture time increased for both cell types. However, A431 cells, preferring gathering together, were confluent on Day 5, while HaCaT cells with better dispersity reached the confluence stage one day earlier (Day 4). Thus, we could deduce that A431 cells grow more slowly than HaCaT cells. The cell growth curves derived from daily cell number counting (Fig. 3C) verified this conclusion. Compared with HaCaT cells, A431 cells were always fewer and exhibited a distinct proliferation rate. The cell number of this cell type increased continuously with an almost constant rate from Day 1 to Day 5. The lower proliferation rate resulted in cell

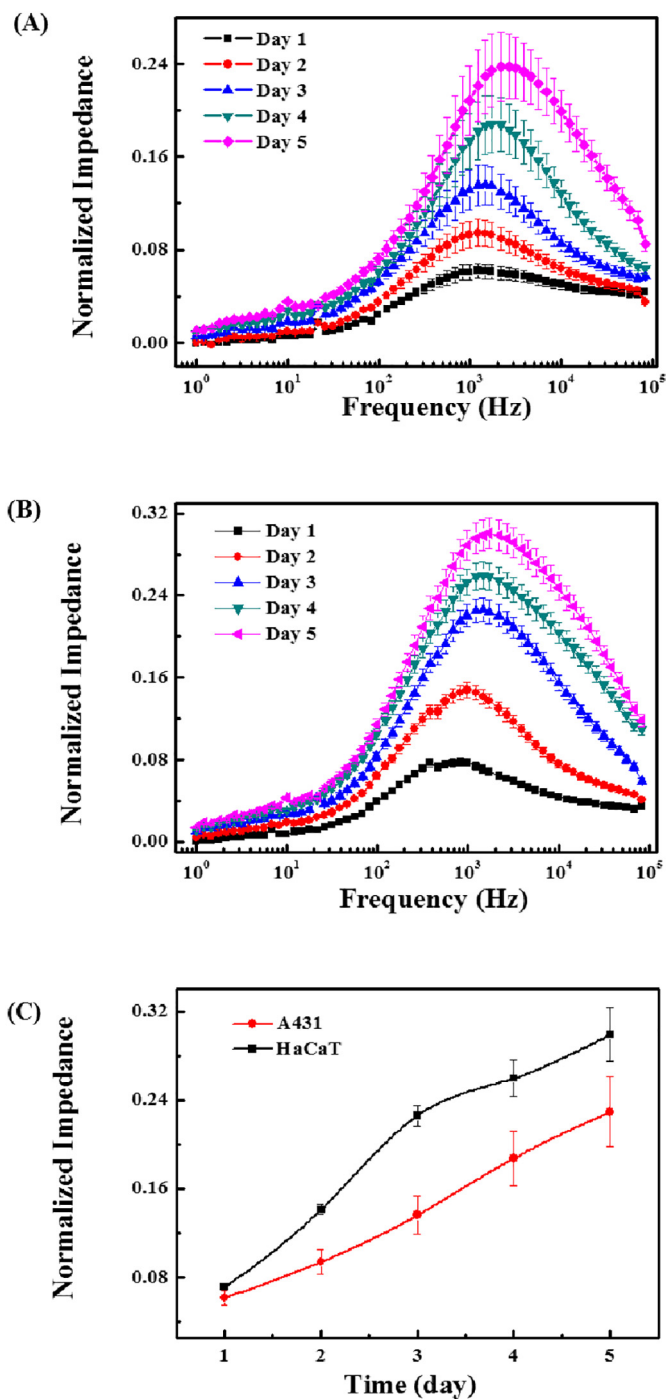


Fig. 2. Normalized impedance curves of (A) A431 and (B) HaCaT cells cultured on ITO glass in the EIS device for 5 days. (C) Normalized impedance curves of A431 and HaCaT cells collected at 1465 Hz as a function of culture time.

confluence on the last day of culture period. In other word, A431 cells were in their exponential growth phase for most of the time. Consequently, the cells kept continuously growing. Additionally, cancer cells showed no contact inhibition. Even the surface of the working electrode was covered; the cells continued to divide, piling up into mounds, leading to the continuous increase in cell number. For HaCaT cells, the cell number increased quickly from Day 1 to Day 3, corresponding to the exponential growth phase. Subsequently, the cell proliferation slowed, corresponding to the stagnating phase. Cells in the exponential growth phase have strong activity and good capability of proliferation. With the increase of cell number, the cells began to contact each other

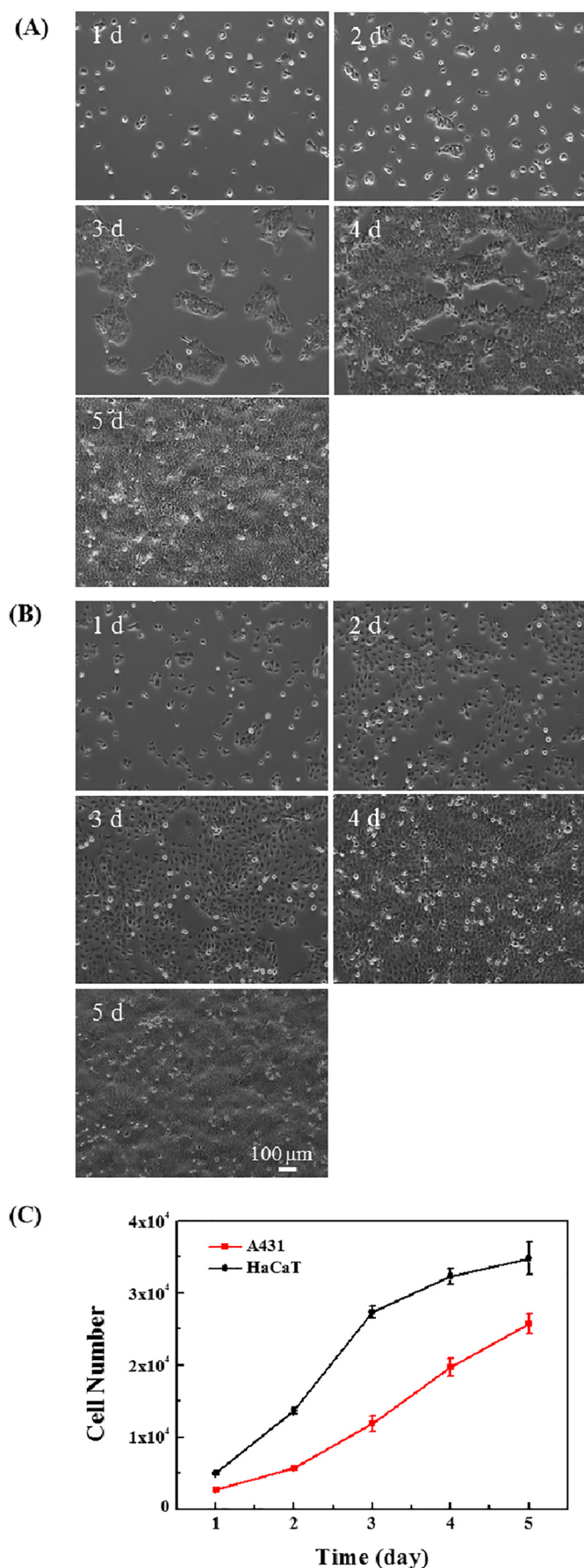


Fig. 3. Microscopic images of (A) A431 and (B) HaCaT cells cultured on ITO glass in the EIS device for 5 days. (C) The growth curves of the two cell types with an initial seeding density of 8000 cells/cm².

and gradually covered all surfaces of working electrode. Due to contact inhibition and density inhibition, cells gradually terminated division and enter the stagnating phase. As a result, HaCaT cells first proliferated fast and then displayed a declined proliferation rate.

Correlating the cell proliferation behaviors to the NI curves in Fig. 2, it was found that the changes in NI values could be a result of the differences in cell proliferation behaviors. The higher NI values of HaCaT cells versus A431 cells were due to the larger cell number. The NI values of A431 cells increased steadily throughout the entire process, which was contributed by the almost unchanged rate of cell proliferation. Meanwhile, HaCaT cells had a relatively faster increase in NI value from Day 1 to Day 3, because the cells multiplied exponentially during this exponential growth phase. After Day 3, the NI value rate increase slowed as they gradually entered the stagnating phase. Consequently, the results of EIS measurement were comparable to those from the microscopic analysis, indicating that EIS is a reliable method to achieve the quantitative monitoring of cell behaviors.

3.2. Distinguishing skin cancer cells and normal cells

To establish the precise discrimination by EIS determination, equivalent circuits were introduced to illustrate the electrical properties of the two cell types in detail with the calculation of their electrical parameters. The impedance spectrum of the system without cells can be represented by an equivalent circuit with two parameters: the solution resistance (R_s) and the double layer capacitance of the electrodes (C_{dl}) (Fig. 4A). When the cells were cultured on the working electrode, the equivalent circuit should contain the impedance contributions from the cells except R_s and C_{dl} (Fig. 4B). The impedance due to the cell proliferation could be modeled as a resistance (R_c) and a capacitance (C_c) related to the cell layer covering the working electrode in parallel [28,29]. Thus, the overall impedance of the system with cells can be expressed as

$$Z = R_s + \frac{1}{j\omega C_{dl}} + \frac{1}{\frac{1}{R_c} + j\omega C_c} \quad (2)$$

where ω is the angular frequency of the electrical signal, indicating that impedance is positively correlated to resistance and inversely correlated to capacitance. The fitting of the recorded impedance data was performed according to the respective equivalent circuits, and the development of fitting curves were realized with the residual sums of squares (χ^2), calculated as 6.06×10^{-3} and 1.57×10^{-3} for the system without and with cells (A431 cells on Day 3, Fig. 4C and D), respectively (Table S1, Supplementary data), indicating that these two equivalent circuits are feasible to represent the EIS measurements.

The values of the electrical components included in the equivalent circuits were calculated by fitting the recorded impedance spectra to the equivalent circuits. Thus, the variation of R_c and C_c could be analyzed during the proliferation processes of the two cell types. First, the simulated values of C_{dl} at 9.82 μ F and R_s at 23.90 Ω were derived according to the equivalent circuit without cells. Next, after fitting the impedance spectra to the equivalent circuit with cells, the simulated values of R_c and C_c were obtained at different time in the culture period with the values of R_s and C_{dl} remaining constant in the equivalent circuit. Importantly, in order to establish the correlation between the electrical properties of the two cell types and their respective proliferation behaviors, the value changes of R_c and C_c were depicted as a function of cell numbers (N) counted from the cell images captured every 24 h during cell proliferation. As shown in Fig. 5A, the R_c values of both A431 and HaCaT cells increased slightly with the increase in cell number over the 5-day culture period. These changes might be

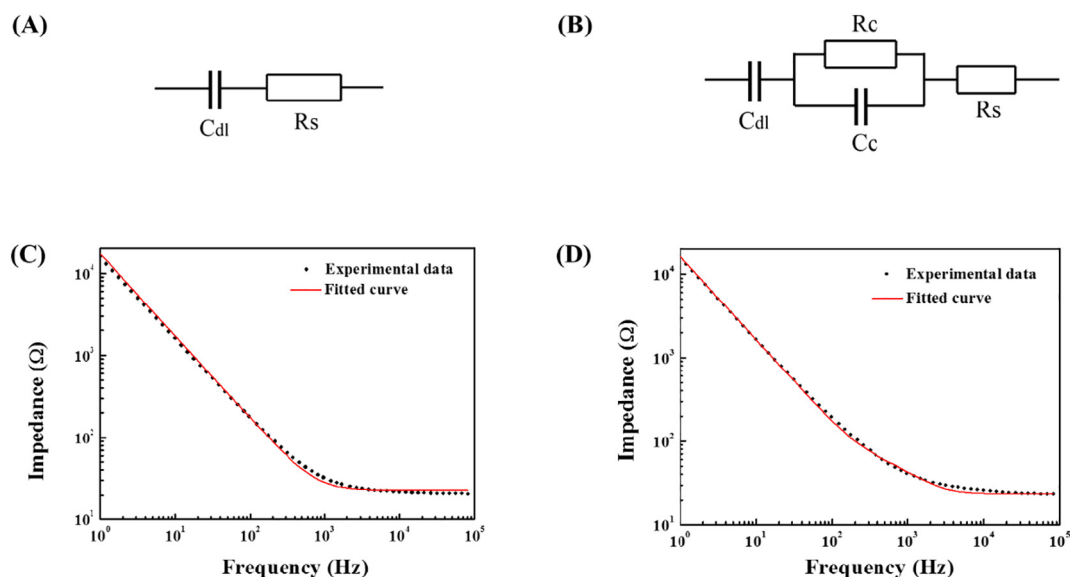


Fig. 4. The equivalent circuits of the impedance measurement system when the cells are absent (A) and present (B) on ITO glass in the EIS device, and the corresponding impedance and fitting spectra to the equivalent circuits without cells (C) and with cells (D). R_s and C_{dl} refer to the solution resistance and the double layer capacitance of the electrodes, respectively; R_c and C_c refer to the resistance and capacitance, respectively, of the cell layer covering on the working electrode.

related to the increased coverage of the electrodes by the cells with their insulating membranes, resulting in the decrease of free electrode surface area and further increased R_c value. However, for A431 cells, the R_c values changed from 11.10Ω to 11.93Ω (an increase of 7.5%). Meanwhile, for HaCaT cells, the R_c values changed from 15.45Ω to 17.44Ω (an increase of 12.9%). Clearly, A431 cells produced smaller R_c values at equal cell numbers and a lower R_c increase rate in comparison with HaCaT cells, due to the relatively smaller proliferation ability of A431 cells, evident by the captured cell images. In addition, no linear relationships could be established between the change of R_c values and the respective numbers of these two cell types.

Corresponding to the slight increases in R_c values, both A431 and HaCaT cells displayed significant decreases in C_c values caused by cell proliferation (Fig. 5B). The C_c values of A431 cells decreased from $26.0 \mu\text{F}$ to $4.5 \mu\text{F}$ (a decrease of 82.7%). Meanwhile, the C_c values of HaCaT cells decreased from $21.8 \mu\text{F}$ to $4.6 \mu\text{F}$ (a decrease of 78.9%). It was observed that these two cell types did not have a very striking difference in C_c values at equal cell numbers compared with R_c values. However, C_c values still had a more obvious distinction between A431 and HaCaT cells at large cell numbers than at small cell numbers. In addition, from Eq. (2), we know that both an increase in R_c and a decrease in C_c could increase impedance. However, the comparison

between the percentage increase of R_c and the percentage decrease of C_c suggests that cell proliferation has more influence on the C_c changes; thus, the decrease in C_c values contribute more to the increased impedance.

More remarkably, there were linear relationships between C_c values and cell number for both A431 and HaCaT cells during the proliferation process, as illustrated in Fig. 5B. The linear relationships for A431 cells and HaCaT cells were $C_c (\mu\text{F}) = -8.05 \times 10^{-4} N (\text{cells}) + 25.1$ with a linear regression coefficient $R = 0.994$, and $C_c (\mu\text{F}) = -5.08 \times 10^{-4} N (\text{cells}) + 22.4$ with a linear regression coefficient $R = 0.982$. These results indicated that the same number increase in A431 cells caused a larger decrease in C_c value compared with HaCaT cells. In other words, the C_c value was more sensitive to the cell number increase of A431 cells. Moreover, based on the correlations between C_c values and cell numbers, quantitative detection of cell numbers for both cell types could be realized in a real-time and continuous manner without the assistance of any imaging methods. In summary, A431 and HaCaT cells presented different resistance and capacitance values and variation trends, establishing the feasibility of distinguishing skin cancer cells and normal cells with the EIS method, which could be a potential diagnostic approach.

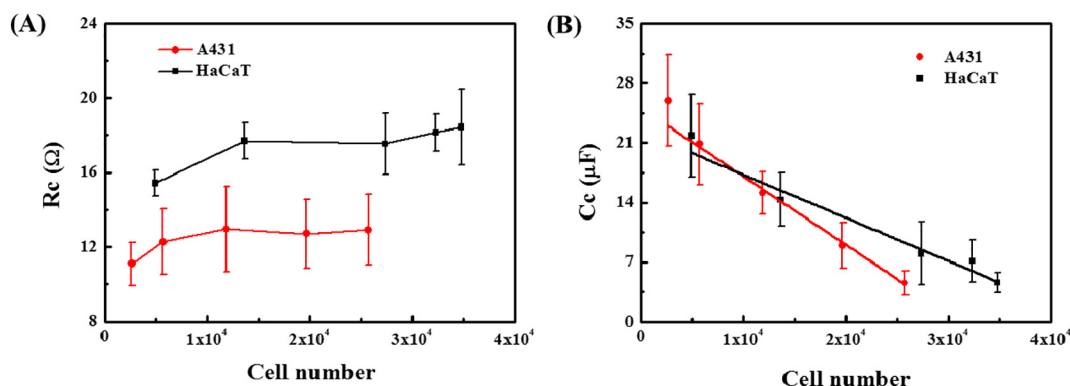


Fig. 5. (A) The correlations between the resistance change and the numbers of A431 and HaCaT cells. (B) The correlations between the capacitance change between the numbers of A431 and HaCaT cells.

4. Conclusions

In this study, electrical impedance spectroscopy was employed to distinguish skin cancer (A431 cells) and normal cells (HaCaT cells) using a novel EIS device with improved sensitivity, reutilization potential and low cost. The time-dependent NI curves of the two cell types at 1465 Hz, the optimum frequency for discrimination, indicated that NI values increased gradually as the cells proliferated in the EIS device over a period of 5 days. However, the increasing rates of NI values for the two cell types were clearly distinct, as confirmed by the simultaneous microscopic imaging, illustrating that A431 and HaCaT cells presented different proliferation behaviors. The resistance and capacitance changes of cells with the increase of cell number during the proliferation process were further researched by the fitting to the established equivalent circuits. A431 cells had smaller R_c values with a smaller increasing variation than HaCaT cells, and the changes of R_c values were non-linearly correlated to the numbers of the two cell types. Meanwhile, A431 and HaCaT cells had comparable C_c values and decreasing variation. Linear correlations were established between the change in C_c values and the cell numbers, allowing us to perform quantitative analysis of these two cell types. Our results demonstrated that the developed EIS system could distinguish A431 cells and HaCaT cells according to the values and variation trends of R_c and C_c extracted in the proliferation process and provide real-time kinetic information of cell proliferation behaviors. The further discrimination of these two cell types is underway in a mixed culture system to promote the practical use of EIS in the early diagnosis of skin cancer cells.

Supplementary data to this article can be found online at <https://doi.org/10.1016/j.jelechem.2018.06.021>.

Acknowledgments

This work was supported by the National Natural Science Foundation of China (Grant No. 21405049).

References

- [1] M.C.F. Simoes, J.J.S. Sousa, A. Pais, Skin cancer and new treatment perspectives: a review, *Cancer Lett.* 357 (1) (2015) 8–42.
- [2] X. Zhang, K. Xiao, L. Cheng, H. Chen, B. Liu, S. Zhang, J. Kong, Visual and highly sensitive detection of cancer cells by a colorimetric aptasensor based on cell-triggered cyclic enzymatic signal amplification, *Anal. Chem.* 86 (11) (2014) 5567–5572.
- [3] J. Chen, H. Jiang, H. Zhou, Z. Hu, N. Niu, S.A. Shahzad, C. Yu, Specific detection of cancer cells through aggregation-induced emission of a light-up bioprobe, *Chem. Commun.* 53 (15) (2017) 2398–2401.
- [4] L. Liang, M. Su, L. Li, F. Lan, G. Yang, S. Ge, J. Yu, X. Song, Aptamer-based fluorescent and visual biosensor for multiplexed monitoring of cancer cells in microfluidic paper-based analytical devices, *Sensors Actuators B Chem.* 229 (2016) 347–354.
- [5] S. Ge, Y. Zhang, L. Zhang, L. Liang, H. Liu, M. Yan, J. Huang, J. Yu, Ultrasensitive electrochemical cancer cells sensor based on trimetallic dendritic Au@PtPd nanoparticles for signal amplification on lab-on-paper device, *Sensors Actuators B Chem.* 220 (2015) 665–672.
- [6] P. Kara, Y. Erzurumlu, P.B. Kirmizibayrak, M. Ozsoz, Electrochemical aptasensor design for label free cytosensing of human non-small cell lung cancer, *J. Electroanal. Chem.* 775 (2016) 337–341.
- [7] M.U.A. Prathap, C.I. Rodriguez, O. Sadak, J. Guan, V. Setaluri, S. Gunasekaran, Ultrasensitive electrochemical immunoassay for melanoma cells using mesoporous polyaniline, *Chem. Commun.* 54 (7) (2018) 710–714.
- [8] R. Pradhan, M. Mandal, A. Mitra, S. Das, Monitoring cellular activities of cancer cells using impedance sensing devices, *Sensors Actuators B Chem.* 193 (2014) 478–483.
- [9] F. Fasbender, C. Watzl, Impedance-based analysis of natural killer cell stimulation, *Sci. Rep.* 8 (2018) 1–9.
- [10] M.D. Rees, S.R. Thomas, Using cell-substrate impedance and live cell imaging to measure real-time changes in cellular adhesion and de-adhesion induced by matrix modification, *J. Vis. Exp.* (96) (2015) 1–8.
- [11] N. Hu, J. Fang, L. Zou, H. Wan, Y. Pan, K. Su, X. Zhang, P. Wang, High-efficient and high-content cytotoxic recording via dynamic and continuous cell-based impedance biosensor technology, *Biomed. Microdevices* 18 (5) (2016) 1–7.
- [12] G.H. Lee, J.-C. Pyun, S. Cho, Electrical impedance characterization of cell growth on interdigitated microelectrode array, *J. Nanosci. Nanotechnol.* 14 (11) (2014) 8342–8346.
- [13] I. Giaever, C.R. Keese, Monitoring fibroblast behavior in tissue culture with an applied electric field, *Proc. Natl. Acad. Sci. U. S. A.* 81 (12) (1984) 3761–3764.
- [14] Y. Xu, X. Xie, Y. Duan, L. Wang, Z. Cheng, J. Cheng, A review of impedance measurements of whole cells, *Biosens. Bioelectron.* 77 (2016) 824–836.
- [15] J. Hong, K. Kandasamy, M. Marimuthu, C.S. Choi, S. Kim, Electrical cell-substrate impedance sensing as a non-invasive tool for cancer cell study, *Analyst* 136 (2) (2011) 237–245.
- [16] H. Zhao, F. Zhang, P. He, Impedance monitoring of SH-SY5Y cell adhesion and responses to As_2O_3 treatment by indium tin oxide microelectrode arrays, *IEEE Sensors J.* 17 (17) (2017) 5426–5430.
- [17] A. Spencer, A.B. Baker, High throughput label free measurement of cancer cell adhesion kinetics under hemodynamic flow, *Sci. Rep.* 6 (2016) 1–10.
- [18] X. Zhang, W. Wang, F. Li, I. Voiculescu, Stretchable impedance sensor for mammalian cell proliferation measurements, *Lab Chip* 17 (12) (2017) 2054–2066.
- [19] N. Tien Anh, T.-I. Yin, D. Reyes, G.A. Urban, Microfluidic chip with integrated electrical cell-impedance sensing for monitoring single cancer cell migration in three-dimensional matrixes, *Anal. Chem.* 85 (22) (2013) 11068–11076.
- [20] L. Liu, X. Xiao, K.F. Lei, C.-H. Huang, Quantitative impedimetric monitoring of cell migration under the stimulation of cytokine or anti-cancer drug in a microfluidic chip, *Biomicrofluidics* 9 (3) (2015) 1–10.
- [21] Y. Cui, Y. An, T. Jin, F. Zhang, P. He, Real-time monitoring of skin wound healing on nano-grooves topography using electric cell-substrate impedance sensing (ECIS), *Sensors Actuators B Chem.* 250 (2017) 461–468.
- [22] R. Pradhan, S. Rajput, M. Mandal, A. Mitra, S. Das, Frequency dependent impedimetric cytotoxic evaluation of anticancer drug on breast cancer cell, *Biosens. Bioelectron.* 55 (2014) 44–50.
- [23] L. Zou, Q. Wang, M. Tong, H. Li, J. Wang, N. Hu, P. Wang, Detection of diarrhetic shellfish poisoning toxins using high-sensitivity human cancer cell-based impedance biosensor, *Sensors Actuators B Chem.* 222 (2016) 205–212.
- [24] Y. Park, H.W. Kim, J. Yun, S. Seo, C.-J. Park, J.Z. Lee, J.-H. Lee, Microelectrical impedance spectroscopy for the differentiation between normal and cancerous human urothelial cell lines: real-time electrical impedance measurement at an optimal frequency, *Biomed. Res. Int.* 2016 (2016) 1–11.
- [25] J.E. Dick, Electrochemical detection of single cancer and healthy cell collisions on a microelectrode, *Chem. Commun.* 52 (72) (2016) 10906–10909.
- [26] M.A. Khayamian, S. Ansaryan, S.R. Tafti, M.S. Nikshoar, M.H. Amiri, M. Baniassadi, M. Abdollah, Ultrasound assisted electrochemical distinction of normal and cancerous cells, *Sensors Actuators B Chem.* 255 (2018) 1–7.
- [27] S. Arndt, J. Seebach, K. Psathaki, H.J. Galla, J. Wegener, Bioelectrical impedance assay to monitor changes in cell shape during apoptosis, *Biosens. Bioelectron.* 19 (6) (2004) 583–594.
- [28] K. Solly, X.B. Wang, X. Xu, B. Strulovici, W. Zheng, Application of real-time cell electronic sensing (RT-CES) technology to cell-based assays, *Assay Drug Dev. Technol.* 2 (4) (2004) 363–372.
- [29] L. Yang, R. Bashir, Electrical/electrochemical impedance for rapid detection of foodborne pathogenic bacteria, *Biotechnol. Adv.* 26 (2) (2008) 135–150.